Neutron Diffraction Study of He Solidified in a Mesoporous Glass

D. Wallacher,[1] M. Rheinstaedter,[2] T. Hansen,[2] and K. Knorr[1]

[1] *Technische Physik, Universität des Saarlandes, D 66041 Saarbrücken, Germany*
[2] *Institut Laue Langevin, F 38042 Grenoble Cedex 9, France*
E-mail: d.wallacher@rz.uni-saarland.de

He embedded in a porous glass has been studied by neutron diffraction. Along the isochoric path studied, about 30% of the pore filling solidify in the bcc structure at 1.7 K and remain in this state down to 60 mK, the minimum temperature of the experiment. The other part of the pore filling is either liquid or an amorphous solid. The behaviour is discussed in terms of a thermodynamic model.

1. INTRODUCTION

The present study was originally motivated by recent torsion pendulum results on ^{4}He solidified in Vycor that showed a reduction of the moment of inertia below about 0.2 K.[1] This observation has been interpreted as superflow analogous to superfluidity, presumably aided by the presence of vacancies. For this reason the present experiment has been carried down to 60 mK. We anticipate that we have not observed any change of the diffraction pattern that can be related to the onset of such a supersolid state. This is perhaps not surprising since the lattice sites contributing to the superflow have been estimated to amount to about 1%, only, which is below the detection limit of a neutron diffraction experiment. Subsequent measurements have in fact shown that supersolidity is not a peculiarity of pore confined He but shows up in bulk He as well,[2] hence future efforts towards an understanding of this intriguing effect will concentrate on the bulk rather than on pore confined solid.

Nevertheless the confinement of solid He in nanometer pores is an interesting topic of its own. For classical van der Waals systems the crystal structure of the pore solid is usually that of the bulk counterpart. Thus

1013

Ar in Vycor glass and other mesoporous matrices shows a powder diffraction pattern that is consistent with the *fcc* structure, except that the peak widths and intensities are affected by the finite size of the crystallites and by stacking faults.[3] There are however drastic effects of pore confinement on the melting and other first order phase transitions. The transition temperatures are reduced and the transitions show hysteresis with respect to cooling and heating. The orientationally ordered low-T Pa3 phase of solid N_2 is even suppressed completely in 7 nm pores.[4]

The melting line of pressurized He in Vycor has been determined in several types of experiments.[5–7] It is shifted to lower T and higher p relative to the bulk state. This is consistent with the findings on the classical systems mentioned above in the sense that pore confinement extends the range of the liquid phase or more generally of the disordered high-T phase.

With the present neutron diffraction experiment we complement the information on pore confined solid He by structural data.

2. EXPERIMENTAL

The experiment has been carried out on the 2-axis diffractometer D20 of the Institute Laue Langevin. The neutron wavelength is 2.417 Å. The diffracted intensity is recorded by a detector array covering diffraction angles 2θ from 20 to 150°.

Three tablets of controlled pore glass ("Gelsil" from Geltech, Orlando, FL) have been inserted into a cylindrical cell made out of aluminium. Gelsil is quite similar to Vycor, the standard porous glass. Both substrates are practically pure fused silica and have an average pore diameter D of 7 nm. For volume sensitive probes such as diffraction, Gelsil gives a superior ratio of the signals from the pore filling and from the matrix, since the porosity is 68%, compared to 30% for Vycor. The free volume in the cell comprises the pore volume V_{pore} and the dead volume $V_{dead} \approx 1/2 V_{pore}$. Diaphragms are set so that the neutron experiment probes mainly the confined He in V_{pore}. There is however a small remainder of bulk He in the neutron beam, namely in the gaps between the glass tablets and the cell walls. This volume, V_{gap}, amounts to about 5% of V_{dead}. The cell was attached to the mixing chamber of a dilution fridge. The cell was held at about 3 K and pressurized with He gas to a nominal pressure p_s of 70 bars with the result that the cell filled with liquid He. Diffraction patterns have been recorded on cooling down to 0.6 K and heating up back to 3 K. Such thermal cycles have been repeated five times, once down to a minimum temperature of 60 mK and about 300 hundred diffraction patterns have been recorded in total. As a result of cooling, the fill line is

eventually blocked by solid He and the thermodynamic conditions of the cell filling change from isobaric to isopycnic (see below). Reference diffraction data that have been taken with no He in the cell serve as background. Finally a cooling/heating cycle down to 1.86 K has been performed at $p_s =$ 20 bar. Since this pressure is below the minimum melting pressure He remains liquid, there is no blocking and the He in the cell is kept under isobaric conditions. The results of this run supply the diffraction pattern of the pore confined liquid.

3. RESULTS AND DISCUSSION

3.1. Structures

The diffraction patterns contain a lot of reflections from the cell walls and the various thermal shields which are easily identified as such from the comparison with the background pattern. Nevertheless the accuracy of the experiment is low in the regions of intense background lines. The strongest contributions of He to the scattered intensity show up in a range of diffraction angles 2θ between 45 and 56°. Figure 1 shows this section of the diffraction patterns as function of T, as obtained on cooling down from 3 K to 60 mK.

The patterns have been decomposed into various Gaussian peaks that can be assigned to three different states of the He in the cell. See Fig. 2 for such a decomposition of the low-2θ-section. There is a broad structure centred at about 51–52° which we interpret, guided by the results obtained at 20 bar, as the first maximum of the structure factor of non-crystalline He. Since V_{gap} is an order of magnitude lower than V_{pore}, most of this feature is due to the pore confined material. The integrated intensity of this component decreases on cooling, while its position and width show just a weak T-dependence (Fig. 3). Since the energy of the scattered neutrons has not been analyzed we cannot distinguish between the dynamic disorder of the liquid and the frozen-in disorder of an amorphous solid.

There are sharper peaks with a width that is resolution limited. They are easily identified as the reflections of the *hcp* solid He.[8] They obviously stem from the bulk solid in the volume fraction V_{gap}. Their intensities vary erratically from cycle to cycle and to a minor degree even within a cycle (Figs. 1 and 2), indicating that the bulk solid was present in the form of larger crystallites and not as a powder. In case such a crystallite is in the perfect reflection position, the corresponding Bragg peak can be relatively strong even though the contributing volume fraction in V_{gap} is small. The apparent 2θ peak positions depend somewhat on the deviation of the orientation of the crystallite relative to the ideal reflection position.
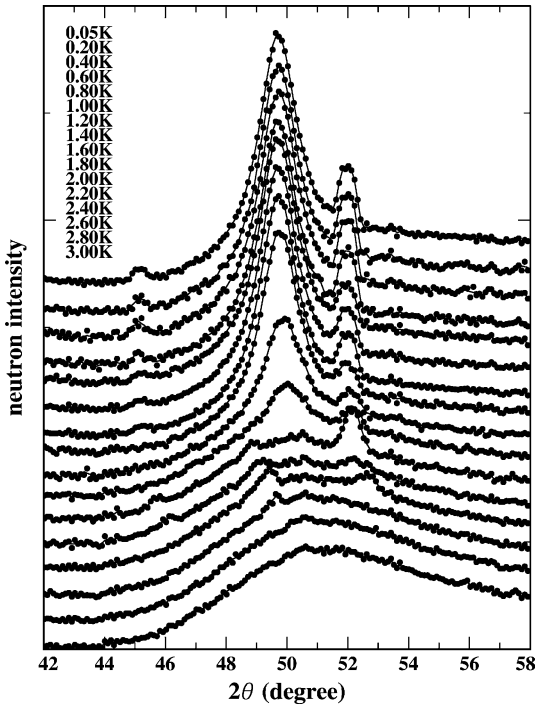
Fig. 1. The low-2θ section of the diffraction pattern for a series of temperatures.

This limits the accuracy of the lattice parameters and of the molar volume of the bulk solid that have been derived from the peak positions (Fig. 3). Nevertheless the bulk solid serves as an internal pressure gauge since the hydrostatic pressure acting on the bulk solid in the cell can be estimated in this way. Reflections of the bulk *bcc* solid have never been observed. From the discussion given further below, it will become clear that the thermodynamic path in the p, T plane did not cross or touch the *bcc* field of the bulk system.

Below 1.7 K an additional peak appears centred at about $2\theta = 50°$. This onset temperature agrees with the previously reported values of the solidification temperature T_f of He in Vycor.[5–7] Hence it represents the pore solid. The width of the peak exceeds the instrumental resolution but is on the other hand significantly smaller than that observed for the non-crystalline component.

This peak is the main piece of evidence for the determination of the structure of the pore solid. We examined four possible structures of the pore confined solid, *hcp*, *fcc*, *bcc* and a random stacking ("*rs*") of
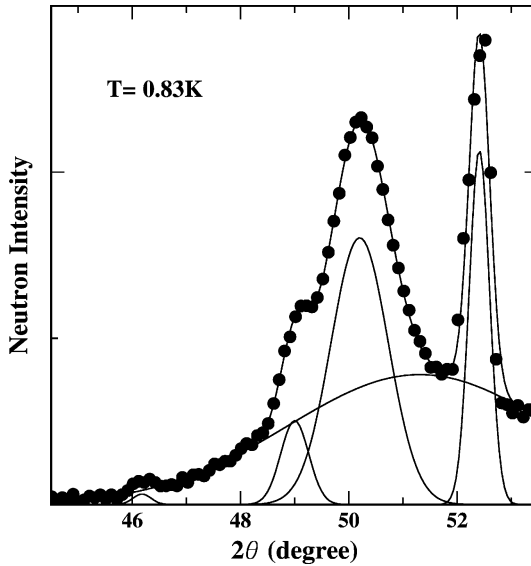
Fig. 2. Decomposition of the diffraction pattern into Gaussians. The peak at 50° represents the *bcc* pore solid, the three sharp peaks are the (100), (002), (101) reflections of the bulk *hcp* solid, the broad feature is the first maximum of the structure factor of the non-crystalline (liquid or amorphous) fraction.

triangular net planes that is a structure intermediate to *hcp* and *fcc*. Stacking faults have been shown to be abundant in the *fcc* Ar pore solid. The pore axes of the porous glass are randomly oriented in space, hence one expects a powder pattern in which at least at lower scattering angles 2θ all powder lines should be present. The *fcc* and the *hcp* structure can be ruled out since they call not only for one but two resp. three peaks in the low-2θ-section of the diffraction pattern, (111) and (200) for *fcc* and (100), (002), (101) for *hcp*. The *rs* and the *bcc* structure meet the criterion of a single Bragg peak at low 2θ, (002) for *rs* (in hexagonal notation) and (110) for *bcc*. Random stacking is however expected to lead to additional scattered intensity that is distributed along (hk) Bragg rods.[9] In a powder pattern this gives rise to asymmetric Warren-type profiles known e.g. from diffraction work on monolayers adsorbed on randomly oriented planar substrates. The absence of such features, in particular of the (10) Warren peak, rules out the *rs* structure. Thus the peak of the pore solid is interpreted as the (110) peak of the *bcc* structure. The next overtone reflections of the *bcc* structure are (200) and (211). The (200) reflection is not visible in our experiments, it is obviously below the detection limit. In a powder diffraction study on the bulk *bcc* solid,[10] the (200)
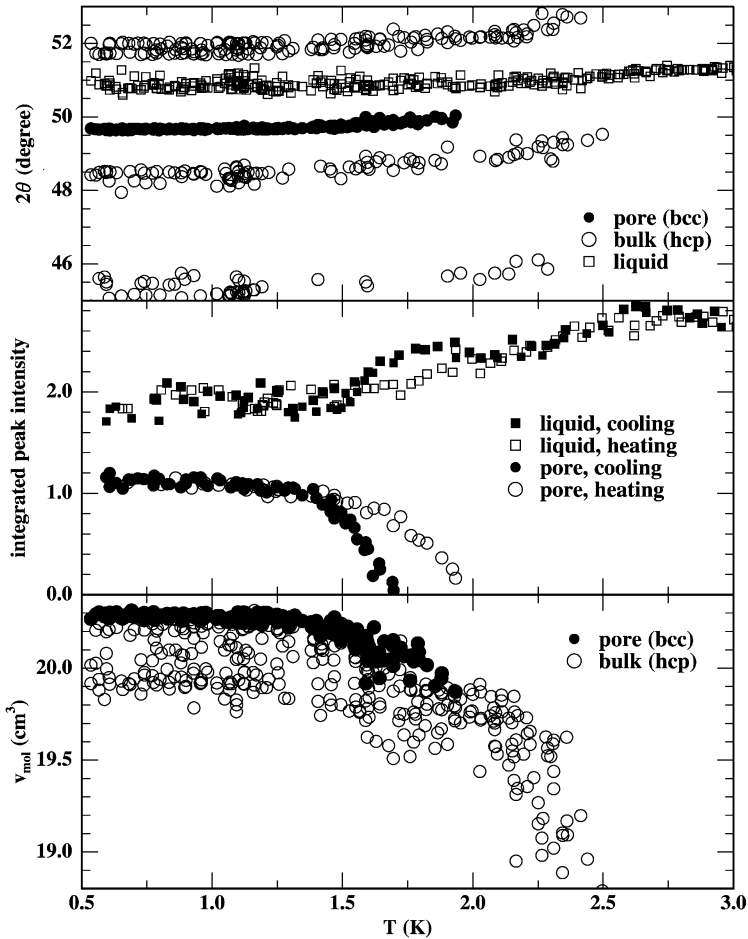
Fig. 3. The *T*-dependence of the peak positions (upper panel), of the integrated intensities of the pore peak and of the non-crystalline component (centre panel), and of the molar volumes of the *bcc* pore solid and of the bulk *hcp* solid (bottom panel).

reflection was said to be "very weak" with respect to (110). The (211) reflection could be identified as a small and relatively broad feature centred at a 2θ-angle of $94°$. The integrated intensities of the (211) peak is 9% of that of the (110) peak. Considering properly the geometric factors of powder diffractometry and the peak multiplicities, this ratio translates into an rms-displacement $<u^2>^{1/2}$ of about 1 Å, a value that is in good agreement with estimates of the zero point motion of solid He.[8] The intrinsic widths ΔQ of the two peaks have been analyzed in terms of the rela-

tion $\Delta Q = 2\pi/L + \Delta a/a Q$, that is as sum of a Q-independent line broadening due to finite crystallite size L and a term linear in the scattering vector Q arising from a distribution Δa of the lattice parameter a. Values of $L = 100$ Å and $\Delta a/a$ of 3% are obtained. L is slightly larger than the pore diameter, obviously the bcc crystallites can grow along the pore axis over distances larger than the pore diameter. Analogous observations have been made on Ar and N_2 in porous glasses. The variation of the lattice parameter a is presumably not so much due to variations of the hydrostatic pressure across pore space but to inhomogeneous strains in the vicinity of lattice defects such as vacancies, dislocations, grain boundaries, and stacking faults that are necessary to adjust the bcc solid to the pore geometry. In the bcc structure the prevailing stacking faults are related to the (211) [111] slip system. Such faults broaden different powder lines to a different extent, $\Delta Q_{(200)}$ being 2.8 times larger than $\Delta Q_{(110)}$.[11] This might be the reason that the (200) line could not be detected.

Diffraction patterns of He solidified in Gelsil with a somewhat smaller pore diameter have been presented recently in context with a study that concentrated on the roton excitations of the pore liquid.[12] The patterns shown in this article are similar to the present ones, but the authors propose that the sharp hcp peaks represent the pore solid.

Figure 3 shows a compilation of the T-dependence of integrated peak intensities and of peak positions, and of the molar volumes of the bulk hcp and of the pore bcc solid as derived from peak positions. As indicated by the T-dependence of the intensity of the (110) peak of the pore solid, the pore filling starts to crystallize on cooling at $T_f = 1.7$ K. Solidification is completed at about 1.4 K. On heating, the melting process is completed at $T_m = 1.9$ K. Thus there is thermal hysteresis between freezing and melting in agreement with previous results on pore confined He.[5–7] Analogous observations have been made on a large number of pore fillings, including the classical van der Waals system Ar.[3] hcp reflections of bulk He (in V_{gap}) are present below 2.5 K. The freezing of the bulk component may actually start at a somewhat higher temperature since the hcp crystallites nucleating first need not be in the reflection position. In fact the non-crystalline component shows a slight decrease on cooling already around 2.6 K. A second and stronger change of the non-crystalline component occurs at temperatures that coincide with T_f on cooling and with T_m on heating. Hence these changes are related to the freezing and melting of the pore material. They are complementary to those of the bcc pore reflection.

The bcc structure of the pore solid exists down to lowest T, quite different to the situation for bulk ^{4}He, but similar to ^{3}He. For the lighter He isotope, it has been argued that the kinetic energy related to the zero point motion is reduced in the bcc structure.[8] Thereby the more loosely

packed *bcc* structure is stabilized relative to the *hcp* structure. The large zero point motion results from a confinement of the He atoms on the length scale of one interatomic distance, the additional confinement in 7 nm-pores with a diameter that corresponds roughly to 20 interatomic distances is not expected to increase the zero point amplitudes significantly. For ^{4}He, the *bcc* structure is observed at higher T, only. Thus for this He isotope the *bcc* structure is stabilized not so much by quantum mechanical effects but by thermal entropy, which in turn is mainly contained in the large thermal amplitudes of TA$_1$ [110] phonons which are known to have relatively low frequencies in the *bcc* structure (not only in *bcc* He but also in *bcc* metals). We think that this situation is not significantly modified by pore confinement either and propose that the *bcc* phase of the ^{4}He pore solid is actually metastable at low T. The *bcc* pore solid forms at higher T as equilibrium state and persists down to lowest T in a metastable state, because the transformation into the stable *hcp* modification is blocked in the pores. Note that there is no group-subgroup relation between the *bcc* and the *hcp* structure, the transition rather requires a reconstruction of the lattice. Such a reconstructive "martensitic" transition can be delayed or even suppressed by lattice defects or opposing boundary conditions. See Ref. 4 for the effects of confinement on the reconstructive β-α transition of N$_2$ and CO in Vycor.

3.2. Thermodynamics

This section deals with the thermodynamic variables temperature T, pressure p and the molar volume v and the phase behaviour of the pore filling. The molar volume of the solidified *bcc* pore solid, v_{bcc}, and of bulk *hcp* He outside the pores, v_{hcp}, are shown as function of T in Fig.3. Note that the volumes are derived from Bragg positions, they may differ from those obtained from thermodynamic measurements. In particular the present values ignore the effects of vacancies.

At some point during the preparation of the cryogenic system for a cooling run, He solidifies in the fill line and the cell is put under isopycnal conditions. (Given the fact that the compressibility and the thermal expansion of the cell walls are negligible compared to He, one can safely refer to isochores in the following). The p, T state of the cell at the moment at which this happens is not known. The first information on the p, T path of the sample is available from the onset of bulk solidification. This occurs at about 2.5 K (see above). The melting pressure of bulk He at this temperature is about 58 bar.[8] On further cooling the isochore follows the bulk melting line until the bulk He in the dead volume has solidified completely. This takes the system down to about 2.25 K and 48 bar, as can be estimated from tabulated data on the molar volumes of the bulk liquid and

the bulk solid on coexistence. This release of pressure causes an expansion of v_{hcp}, in agreement with the experimental results. Thereafter the isochore leaves the bulk melting line, crosses the *hcp* field of the bulk solid until the solidification of the pore filling starts at $T_f = 1.7$ K. The pressure relaxation of this section (about 9 bar) can be roughly estimated from the change of v_{hcp} (about 0.7 cm^3) in this T-interval (Fig.3), by referring again to thermodynamic data.[8] This takes the pressure in the cell to an estimated low-T value of 38 bar. The experimentally observed low-T value of v_{hcp} is (20.1 ± 0.1) cm^3, which translates into a pressure of $p_0 = (37 \pm 1)$ bar acting on the bulk solid outside the pores. This is in conspicuous agreement with the above estimate of the isochoric p, T path down to the point where pore solidification starts. The data of $v_{hcp}(T)$ of Fig. 3 suggest that the subsequent freezing of the pore filling does not lead to a further decrease of the pressure outside, presumably because the pore space is blocked off by solidification of the pore filling, such that isochoric conditions have to be imposed on the pore filling and the bulk solid outside separately.

The molar volume of the *bcc* pore solid is 20.3 cm^3 at low T. In bulk He the *bcc* phase exists in narrow crescent shaped field of the p, T plane extending from 1.4 to 1.7 K at pressures around 28 bar with a maximum p-width of slightly less than 1 bar.[8] On average the molar volume of bulk *bcc* is 0.2 cm^3 larger than that of bulk *hcp*. About the same difference Δv is now encountered between the *bcc* pore filling and the bulk *hcp* material outside the pores at low T. This suggests that the pressure acting on the *bcc* solid inside and on the *hcp* material outside the pores is about the same, that the pressure difference across the pore mouths is less than 1 bar. We will comment on this point later.

The diffraction results clearly show that only the smaller part of the pore filling freezes into the *bcc* crystalline state, the material remaining stays liquid or forms an amorphous solid. The crystalline fraction f_x can be estimated from the ratio of the integrated intensities of the (110) *bcc* reflection and of the peak representing the non-crystalline material, or alternatively from the reduction of the intensity of the latter peak upon crystallization of the pore filling. At low $T, T < 1.4$ K, one arrives at values of f_x between 0.25 and of 0.35. Thinking in terms of well defined phase boundaries, the incomplete liquid–solid transformation means that the pore filling settles at low T just on the pore melting line. In fact the value of p_0 cited above is in agreement the low-T melting pressure of He in Vycor of previous studies. The actual situation is more complicated. The porous glasses are known to have a relatively broad distribution of pore diameters D, $\Delta D / D$ being of the order of 0.3, as suggested by the adsorption branch of sorption isotherms.[3] The liquid–solid boundary of

the pore filling is not a line but a band in the p, T plane. The width of this band can be estimated from the downward shift ΔT of the melting temperature with respect to the bulk system that scales with D^{-1}. This has not only been shown experimentally by studies on substrates with different average pore sizes but also comes out of thermodynamic models that are based on a competition of volume free energies and interfacial energies (see below for such a model). This scaling can be carried over onto the shift of the melting pressure. Accordingly the pore melting pressure should be distributed over a range from about 35 to 40 bars at low T. The material in sections of pore space with large pore diameters is the first to freeze and the last to melt and it has been proposed to derive the pore size distribution from the melting behaviour.[5] Applied to the present system, this view suggests that only the material in the largest pores, which amount to about 30% of pore space, does actually solidify. Calorimetric studies on a large variety of pore fillings show asymmetric melting and freezing anomalies with a long wing towards lower T and an abrupt drop towards higher T, see Ref.13 for Ar. It would need rather peculiar pore size distributions to explain this shape. Hence we think that the phase transformations in pore sections of different diameter do not progress independently, that the liquid and the solid fraction do not primarily coexist in different sections along the pore axes, but in shells at different radial distances R from the pore axis. This symmetry is imposed by the attractive potential U between the He atoms and the cell walls. The "inert" layers on the pore walls, observed e.g. in studies of the superfluidity of He films adsorbed in Vycor,[14] in diffraction work of Ar in Vycor[3] as well as the initial stages of sorption isotherms[14] on porous substrates are manifestations of the radial organization of the pore filling. In a cylindrical pore U depends on a single spatial coordinate, namely $r = R/R_0$, R_0 is the pore radius. We have recently developed a simple thermodynamic model for the melting process in pores[13] based on cylindrical liquid–solid interface. In case the surface excess δ is positive, $\delta = \gamma_{sw} - (\gamma_{sl} + \gamma_{lw})$, the γ's are interfacial energies, the subscripts stand for liquid, solid and wall, the solid does not wet the walls and an intruding liquid shell between the solid in the pore centre and the cell walls forms instead. Due to the competition of the surface excess and the volume free energy, the liquid–solid transformation of the pore filling is then displaced from the bulk melting line and is hysteretic. At the transition a solid core in the pore centre appears that has a finite radius r_c, $0 < r_c < 1$. Applied to the present case the model can reproduce the shift of the melting line, the hysteresis between melting and freezing as well as the solid volume fraction f_x observed in the experiment with δ-values around 0.144 erg/cm^2. Given the fact that $\gamma_{sl} = 0.16$ erg/cm^2,[15] such a value appears realistic.

Based on this discussion, we propose that the pore material at low T is organized as follows: The pore radius R_0 corresponds to about ten monolayer shells. The inner five are crystalline *bcc*, the two next to the walls are "inert" in the sense that they do not support the melting transition, leaving the third to fifth for the liquid state. Doubling the *p*- or *T*-offset relative to the bulk melting line is estimated to reduce the liquid shell to one monolayer. This may be still enough for 2D superfluidity to occur below about 200 mK. (Note however that the model relies on a high-T expansion and treats the pore filling as continuum rather than as series of individual monolayers).

We close this section with remarks on the radial pressure gradient in the pore. The potential $U(r)$ exerts a hydrostatic pressure on the pore filling. For cylindrical symmetry U is a hypergeometric function of r, the strength of the potential of He interacting with glass walls is approximately known.[16] Already in the pore centre ($r = 0$) the pressure is larger than that of the bulk solid outside, by about 0.5 bar. This small pressure difference is consistent with experimental data. The hydrostatic pressure increases with increasing r and reaches 1.4 bar at $r = 0.5$ and 240 bar at $r = 0.1$ i.e. at a distance from the wall that corresponds to the thickness of one monolayer. This latter value is academic since the micro-roughness of the glass walls has to be considered. Nevertheless the hydrostatic pressure squeezes the "inert" layers next to the walls into a disordered state. Finally the capillary pressure γ_{sl}/R related to the curved liquid–solid interface has to be considered. For a cylindrical interface at $r = 0.5$ the pressure difference across the interface is estimated to be about 0.9 bars.

4. SUMMARY

Due to the pore confinement the melting transition is shifted to lower temperatures and higher pressures. There is hysteresis between freezing and melting. The present diffraction study identifies the structure of the pore solid as *bcc*. The *bcc* state extends down to lowest temperatures in marked contrast to bulk He. We suggest that this not so much due to the fact that the *bcc* phase is a stable low-T modification of pore confined He, but that the martensitic transformation into the *hcp* phase is blocked due to abundant lattice defects that are necessary to adapt the solid to the pore confinement. For the thermodynamic path of the present experiment, crystallization is incomplete, about 70% of the pore filling are non-crystalline. The non-crystalline fraction presumably consists of about two monolayers of immobile molecules next to the pore walls and a liquid-like shell between this wall coating and the crystalline core in the pore centres. Indications of a supersolid phase have not been detected.

ACKNOWLEDGMENTS

REFERENCES

1. E. Kim and M. H. W. Chan, *Nature* **427**, 225 (2004).
2. E. Kim and M. H. W. Chan, *Scienc*e **305**, 1941 (2004).
3. P. Huber and K. Knorr, *Phys. Rev. B* **60**, 12657 (1999).
4. P. Huber, D. Wallacher, and K. Knorr, *Phys .Rev. B* **60**, 12666 (1999).
5. E. D. Adams, K. Uhlig, Y. H. Tang, and G. E. Haas, *Phys. Rev. Lett.* **52**, 2249 (1984).
6. J. R. Beamish, A. Hikata, L. Tell, and C. Elbaum, *Phys. Rev. Lett.* **50**, 425 (1983).
7. C. Liezhao, D. F. Brewer, C. Girit, E. N. Smith, and J. D. Reppy, *Phys. Rev. B* **33**, 106 (1986).
8. Thermodynamic and structural data on bulk He can be found in *Rare Gas Solids*, M. L. Klein, and J. A. Venables eds., Academic Press, London (1977), chapter 7, p. 382 by H. R. Glyde and chapter 11, p. 663 by R. K. Crawford.
9. B. E. Warren, *X-Ray Diffraction*, Addison-Wesley, Reading, MA, (1969).
10. A. F. Schuch and R. L. Mills, *Phys. Rev. Lett.* **8**, 469 (1962).
11. O. J. Guentert and B. E. Warren, *J. Appl. Phys.* **29**, 40 (1958).
12. J. V. Pearce, J. Bossy, H. Schober, H. R. Glyde, D. R. Daughton, and N. Mulders, *Phys. Rev. Lett.* **93**, 145303 (2004).
13. D. Wallacher and K. Knorr, *Phys. Rev. B* **63**, 104202 (2001).
14. R. H. Tait and J. D. Reppy, *Phys. Rev. B* **20**, 997 (1979).
15. S. Balibar, D. O. Edwards and C. Laroche, *Phys. Rev. Lett.* **42**, 782 (1979).
16. W. F. Saam and M. W. Cole, *Phys. Rev. B* **11**, 1086 (1975).